crystals

MDPI

Article

Effect of Fe and Thermal Exposure on Mechanical Properties of Al-Si-Cu-Ni-Mg-Fe Alloy

Jingdong Li [1], Fanming Chen [2], Yuze Wang [2], Yuanliang Zhang [2,*], Rui Zhang [1], Yi Luo [2], Yiqiang He [2], Ke Sun [2] and Lijie Zuo [2,*]

[1] Jiangsu Institute of Automation, Lianyungang 222061, China
[2] Jiangsu Institute of Marine Resources Development, Jiangsu Ocean University, Lianyungang 222005, China
* Correspondence: zhangyl@jou.edu.cn (Y.Z.); zuoliji@126.com (L.Z.)

Abstract: The effects of Fe, Cr and thermal exposure on the microstructure and mechanical properties of Al-Si alloy were investigated in this work. The results indicated that the main phases of the Al-Si-Cu-Ni-Mg-(0.6–0.9%) Fe (wt. %) alloy were α-Al, Si, $Al_5Cu_2Mg_8Si_6$, Al_3CuNi, Al_7Cu_4Ni, Al_2Cu, and AlFeSi at room temperature. The size of the AlSiFe phase increased with increasing the weight fraction of Fe. The shape of Fe-rich phase changed from rod-like to star-like, followed by long needle-like with Fe varying from 0.6% to 0.9%. The mechanical properties of the studied alloys at elevated temperatures increased with Fe. The ultimate tensile strength of the three alloys at 350 °C was 111.2 MPa, 124 MPa, and 128.7 MPa, respectively. In addition, the ductility and strength of the studied alloys at room temperature decreased with increasing the Fe, due to the large size of the hard and brittle Fe-rich phase strictly cleaved the aluminum matrix. After thermal exposure, the properties of the alloy at room temperature and elevated temperature decreased obviously at the beginning of 0.5~8 h, and then tend to be stabilized during thermal exposure at 350 °C for approximately 32~64 h. Fe-rich was a thermal stable phase at 350 °C.

Keywords: Al-Si alloy; heat-resistant aluminum alloy; microstructure; mechanical properties

check for updates

Citation: Li, J.; Chen, F.; Wang, Y.; Zhang, Y.; Zhang, R.; Luo, Y.; He, Y.; Sun, K.; Zuo, L. Effect of Fe and Thermal Exposure on Mechanical Properties of Al-Si-Cu-Ni-Mg-Fe Alloy. *Crystals* **2023**, *13*, 993. https://doi.org/10.3390/cryst13070993

Academic Editors: Umberto Prisco and Hongbin Bei

Received: 14 May 2023
Revised: 14 June 2023
Accepted: 16 June 2023
Published: 21 June 2023

Copyright: © 2023 by the authors. Licensee MDPI, Basel, Switzerland. This article is an open access article distributed under the terms and conditions of the Creative Commons Attribution (CC BY) license (https://creativecommons.org/licenses/by/4.0/).

1. Introduction

As the fundamental components of an engine, pistons must exhibit exceptional wear resistance and high-temperature performance. Meeting the service conditions with the general Al-Si alloy can be difficult; meanwhile, the heat-resistant Al-Si alloy has obvious advantages. Heat-resistant aluminum alloy has a good high-temperature performance, high-temperature lasting strength and thermal stability. However, with the continuous development of the engine, the service conditions can gradually become harsher. Pistons usually work at more than 300 °C and need to bear alternating loads. As displayed in Table 1, the mechanical properties of Al-Si alloys measured at 350 °C were reported by literatures. The mechanical properties of the piston decline sharply during the service process, leading to fatigue failure. Therefore, it is urgent to develop a type of heat-resistant Al-Si alloy with more stable high-temperature endurance strength to meet the increasingly harsh service environments of the engine.

Meng et al. [1] found that the T-AlFeNi phase possessed excellent high-temperature performance in Al-12Si alloy with different Fe/Ni ratios; meanwhile, the UTS reached up to 106 MPa at 350 °C. Compared with the alloy without the T phase, the increase rate was up by 23%. Farkoosh [8] found that Q-$Al_5Mg_8Cu_2Si_6$ was the main heat-stable phase at 300 °C. With the Mg concentration increased from 0.3 wt. % to the maximum solubility of 0.5 wt. %, the content of Q-phase increased from 0.9% to 1.5%. Q-$Al_5Mg_8Cu_2Si_6$ prominently enhanced the tensile strength and creep resistance at 300 °C, but the elongation decreased. Li. [9] studied the microstructure and mechanical properties of the Al-12Si-3.5Cu-2Mn heat-resistant alloy at different temperatures. The results showed that the

addition of Cr optimized the morphology of the primary Mn-rich phase, and the morphology transformed into an elongated rod, followed by dendrite, and finally star particles; the volume fraction of the Mn-rich phase increased distinctly. The Cr element mainly dissolved in the primary Mn rich phase and a small amount in the matrix. No new Cr rich phase formed in the alloy. The addition of Cr dramatically advanced the strength and elongation of the alloy at room temperature and high temperature. Zhang [10] investigated the effect of thermal exposure on the microstructure and mechanical properties of the Al-Si-Cu-Ni-Mg alloy with different casting processes of PMC (metal mold casting) and HPDC (high pressure die casting) at 350 °C for 200 h. It was found that the Si particles of the two alloys became larger and tended to be spherical without sharp edges, indicating that the eutectic Si was unstable at 350 °C after thermal exposure. Compared with cast alloys, the tensile strength of the alloys after thermal exposure decreased, and the ductility increased due to spheroidization and coarsening of eutectic Si at 350 °C. The tensile strength of TEPMC and TEHPDC alloys was approximately 67 MPa at 350 °C. Due to the coarsening of eutectic Si, the TEPMC alloy possessed better creep resistance than the TEHPDC alloy. Tensile properties and hardness decreased significantly after thermal exposure at 250 °C [11]. A significant reduction in yield strength and an increase in ductility values were observed. During thermal exposure, the distance between the precipitates increased, resulting in the deterioration of the mechanical properties observed after 250 °C exposure to the first 100 h. However, the strength and hardness values did not decrease significantly during the further 200 h of thermal exposure. Zhao [12] reported that the increase in YS (yield strength) after ageing was attributed to the nanometer precipitated phase, which was separated from the α-Al matrix. After thermal exposure at 350 °C for 100 h, the majority of these precipitated phases dissolved in α-Al matrix; fracture and coarsening occurred in the ultra-fine eutectic Si network, resulting in a decrease in YS to 117 MPa and an increase in elongation to 10.3%. Lin [13] illustrated that the mechanical properties of the alloy at elevated temperature were improved with the increase in Ti and Cu, due to an increase in the number of precipitated particles. After thermal exposure at 300 °C for 10 h, the tensile properties decreased, which was attributed to reinforced precipitates coarsened.

Table 1. The elevated temperature performance of partially cast Al-Si alloy in service at 350 °C.

Composition (wt. %)	State	UTS (MPa)	Elongation (%)
Al-11.98Si-4.02Cu-1.02Mg-2.68Ni-0.62Fe [1]	/	106	5.4
Al-12.5Si-5.0Cu-0.84Mg-2.0Ni-0.5Fe [2]	T5	94.4	8.6
Al-11.79Si-3.38Cu-2.05Mn-1.0Cr-0.17Fe [3]	T6	106	8.8
Al-13Si-3.7Cu-3.2Ni-1.1Mg-0.8Fe-0.5Cr [4]	T6	98.61	/
Al-12Si-4Ni-0.9Cu-0.8Mg [5]	/	116	2.0
Al-11.97Si-3.79Cu-0.82Mg-3.39Ni-0.5Fe-0.18Mn-0.1Ti [6]	T7	76.1	9.1
Al-12Si-3Cu-1.5Ni [7]	Cast	61.4	4.8

The introduction of the Fe phase would effectively improve the performance of the studied alloy at 250 °C. Tensile properties and hardness values decreased significantly after thermal exposure at 250 °C. Fe-rich phase was introduced into the Al-Si-Cu-Ni-Mg alloy and the temperature was raised to 350 °C based on previous studies [4,11,13]. In this work, the effect of Fe and thermal exposure on microstructure and mechanical properties of Al-Si-Cu-Ni-Mg-Fe alloy were investigated. The Cr and Sr elements ware used to modify the heat-resistant Al-Si-Cu-Ni-Mg-Fe Alloy. Then, the size of Fe-rich and small size Si was quantitative characterized as-cast and after thermal exposure at 350 °C. The evolution of hardness and ultimate tensile strength of the studied alloys were characterized during thermal exposure at 350 °C for 200 h, which may provide a theoretical basis for developing new high strength and toughness heat-resistant alloys.

2. Experiment

The chemical composition of the designed alloys was shown in Table 2. Before melting, the master alloy, mold, and crucible were kept at 200 °C for 2 h. During the melting process, pure Al was first heated in the resistance furnace until melting, and then Al-Cu, Al-Si and other master alloys were added until the metals became molten at 720 °C, and then heated to 750 °C, Al-Fe master alloy was added until melting completely. Finally, pure Mg wrapped by aluminum foil was added into the crucible, and the Mg block was pressed into the solution with a scraping spoon. Then, the melt was fully stirred to ensure the uniform composition of the alloy. After the stirring, the preheated refining agent C_2Cl_6 was added to refine at 730 °C, and the refining agent was stirred clockwise for approximately 5 min for skimming and degassing. After fully stirring, it was poured into the preheated mold for casting.

Table 2. Chemical composition of cast Al-Si alloy.

Alloys (wt. %)	Si	Cu	Ni	Mg	Fe	Ti	Sr	Cr	Al
Alloy 1	12	3.8	2	0.8	0.3	0.2	0.2	0.5	Bal
Alloy 2	12	3.8	2	0.8	0.6	0.2	0.2	0.5	Bal
Alloy 3	12	3.8	2	0.8	0.9	0.2	0.2	0.5	Bal

The metallographic observation of the sample was carried out on AxiocamMR5 equipment. The selected part of the sample was the middle part of the bottom of the casting. The sample was polished by 320#, 600#, 1000#, 3000# sandpaper, respectively, and then polished on the metallographic polishing machine PG-2B, and the last step was polished on the chamois cloth. Keller's reagent was used for 15 s etching, which was immediately washed with water and sprayed with alcohol for drying.

X-ray diffraction was performed on X'Pert PRO MPD equipment with Cu target, the experimental voltage, test angle, and scanning speed were 40 kV, 5–90°, and 5°/min, respectively. The scanning electron microscopy were American FEI Scios 2 HiVac and Phenom ProX. The dimensions of the tensile samples were shown in Figure 1. Tensile test was carried out on a universal test machine with sample thickness of 2 mm and tensile rate of 2 mm/min at room temperature. The high-temperature instantaneous tensile property was measured by the high-temperature electronic universal testing machine, the sample thickness was 3mm, and the measurement temperature was set at 350 °C, the temperature error was ±2 °C. The temperature was heated to 350 °C and held for 10 min before stretching with a tensile rate of 2 mm/min. The results of tensile at room temperature and high temperature were taken from the average values of 3 parallel samples. The hardness test was performed on a Vickers hardness meter, and the final result was the average of the hardness at seven different points. The thermal exposure specimens were kept in a GSL1400X tubular furnace with a temperature error of ±2 °C and then air cooling. The thermal exposure temperature was 350 °C and varied from 0 to 200 h.



Figure 1. Shape and size of tensile specimens: (**a**) at room temperature, (**b**) at high temperature.

3. Results and Discussion

3.1. Microstructure

As displayed in Figure 2, the alloys were mainly composed of Al matrix, primary Si, eutectic Si, AlFeSi phase and Al_3CuNi phases. The diffraction peak intensity of AlFeSi phase in Alloy 1 to Alloy 3 alloys increased gradually, indicating that the content of AlFeSi phase in studied alloys increased with the Fe.

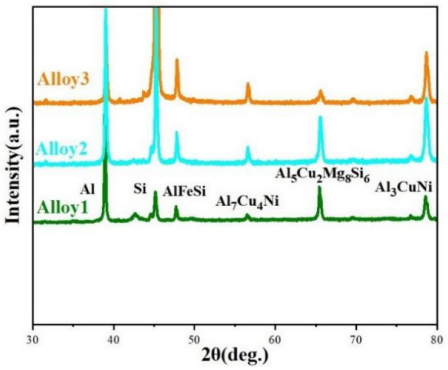


Figure 2. XRD diffraction peak and calibration of cast Al-Si alloy.

The metallographic of the as-cast Al-Si alloy was shown in Figure 3. As displayed in Figure 3a, the mesh phases and fishbone phases were uniformly distributed, and primary Si and black short rod-like AlFeSi phases were also observed. In Figure 3b,c, with the increase in Fe element, Fe-rich phase showed a trend of increasing size and slight aggregation, and the morphology changed into star-shaped. The low-magnification metallographic morphology after thermal exposure was shown in Figure 4, which showed no obvious change compared with that in as-cast alloys.

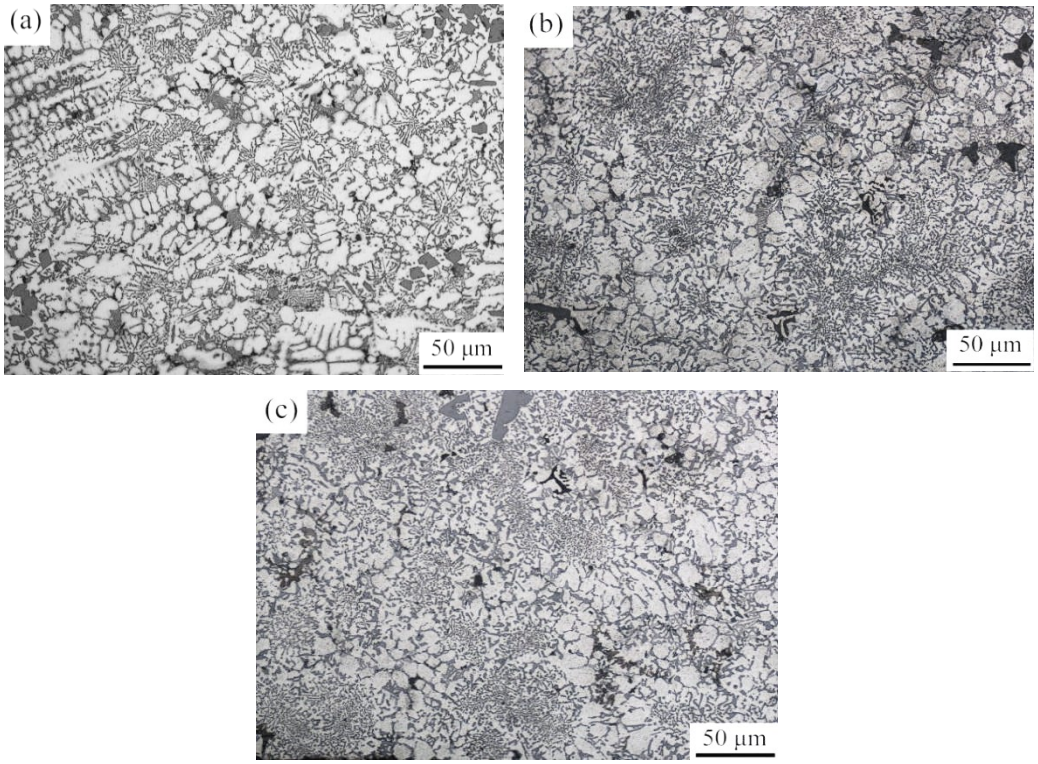


Figure 3. Microstructure of as-cast alloys at low magnification: (**a**) Alloy 1, (**b**) Alloy 2, and (**c**) Alloy 3.

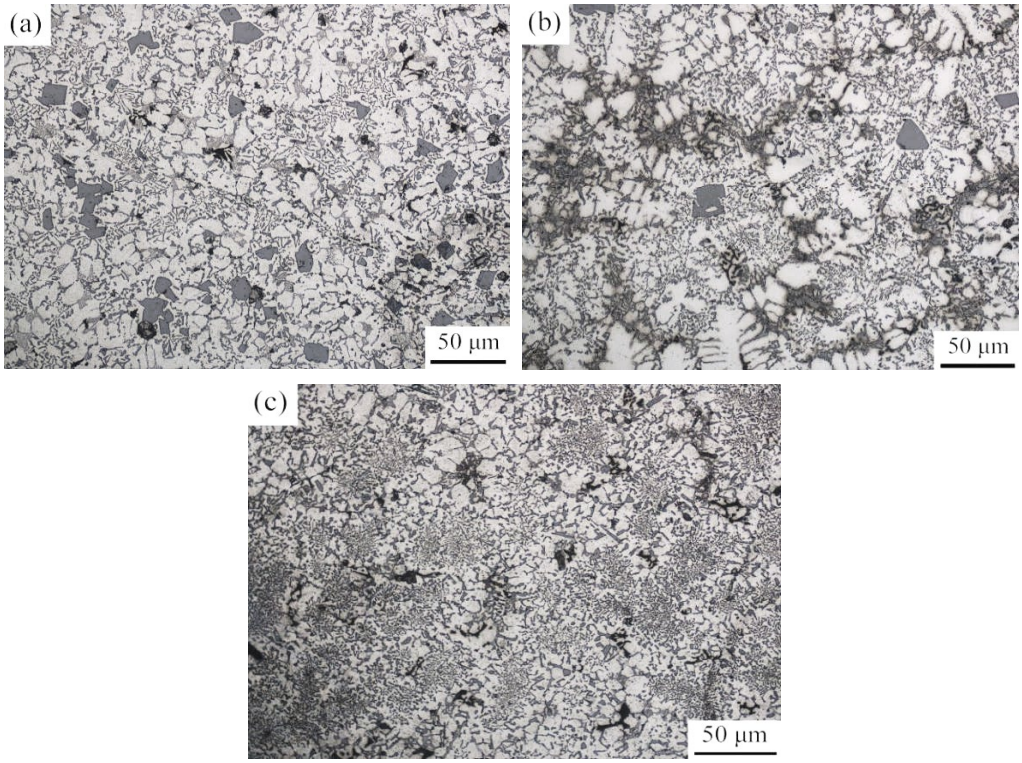


Figure 4. Microstructure of the Al-Si alloy after thermal expose: (**a**) Alloy 1, (**b**) Alloy 2, and (**c**) Alloy 3.

Figure 5 presented the morphologies and EDS calibration of the Fe-rich phases in different alloys. It was detected that Fe-rich phases were AlFeSiCuNi, AlSiFeNi, and AlSiCrFe phase, respectively. The shape of AlFeSiCuNi phase was Chinese characters, and its size was small and short. This five-element phase has been reported in many studies [14,15]. The shape of AlSiFeNi phase was star-like with sharp edges and corners, which tended to induce stress concentration and weaken the mechanical properties of the alloys at room temperature. The phase of AlSiCrFe was found in the alloy. The addition of the Cr element formed the AlSi(Cr, Fe) phase, which optimized the sharp morphology of Fe phase and improved the mechanical properties of the alloy.

Figure 6 demonstrated the SEM morphology and EDS analysis of Q-$Al_5Cu_2Mg_8Si_6$ phase before and after thermal exposure, and Figure 7 displayed the SEM morphology and EDS analysis of Al_3CuNi and Al_2Cu after thermal exposure. As displayed in Figure 6, serious coarsening and spheroidization occurred in the Q phase after thermal exposure, and the shape changed into short rod-like and spherical granular. Moreover, the distribution of the Q phase became more homogeneous, indicating the phenomenon of Q phase dissolution and re-growth occurred during the thermal exposure at 350 °C. The Mg atom percentage of the Q phase was 44.30, higher than the value of 40.30 in Figure 6b, which also confirmed this point.

As shown in Figure 7a, the white bone phase was the Al_3CuNi phase, and the gray rod-shaped phase was the Al_2Cu phase. Before thermal exposure, the Al_3CuNi phase was small in size and dispersed. From Figure 7b,c, it was found that the boundary of the Al_3CuNi phase was blurred after thermal exposure. It was speculated that dissolution occurred during thermal exposure. The coarsening of the Al_2Cu phase occurred to a certain extent after thermal exposure, because the Al_2Cu phase was stable below 250 °C [16,17].

Figure 8 illustrated the surface scanning morphology of Alloy 2 before and after thermal exposure. The distribution of Al, Si and Cu elements showed no significant change, while Ni and Mg elements were slightly aggregated after thermal exposure for Alloy 2. The distribution of the Ti and Cr elements changed from the uniform distribution to the segregation.

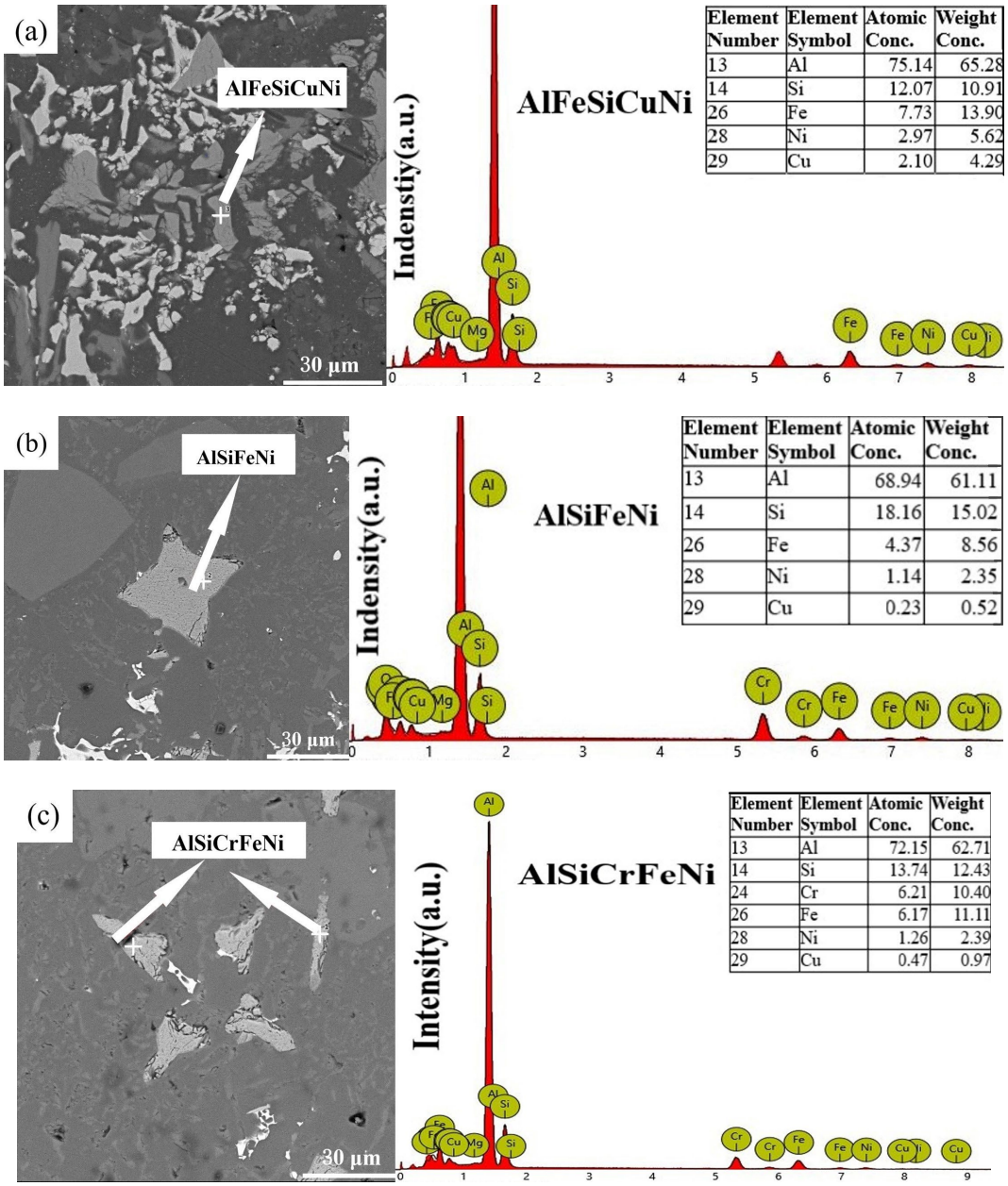
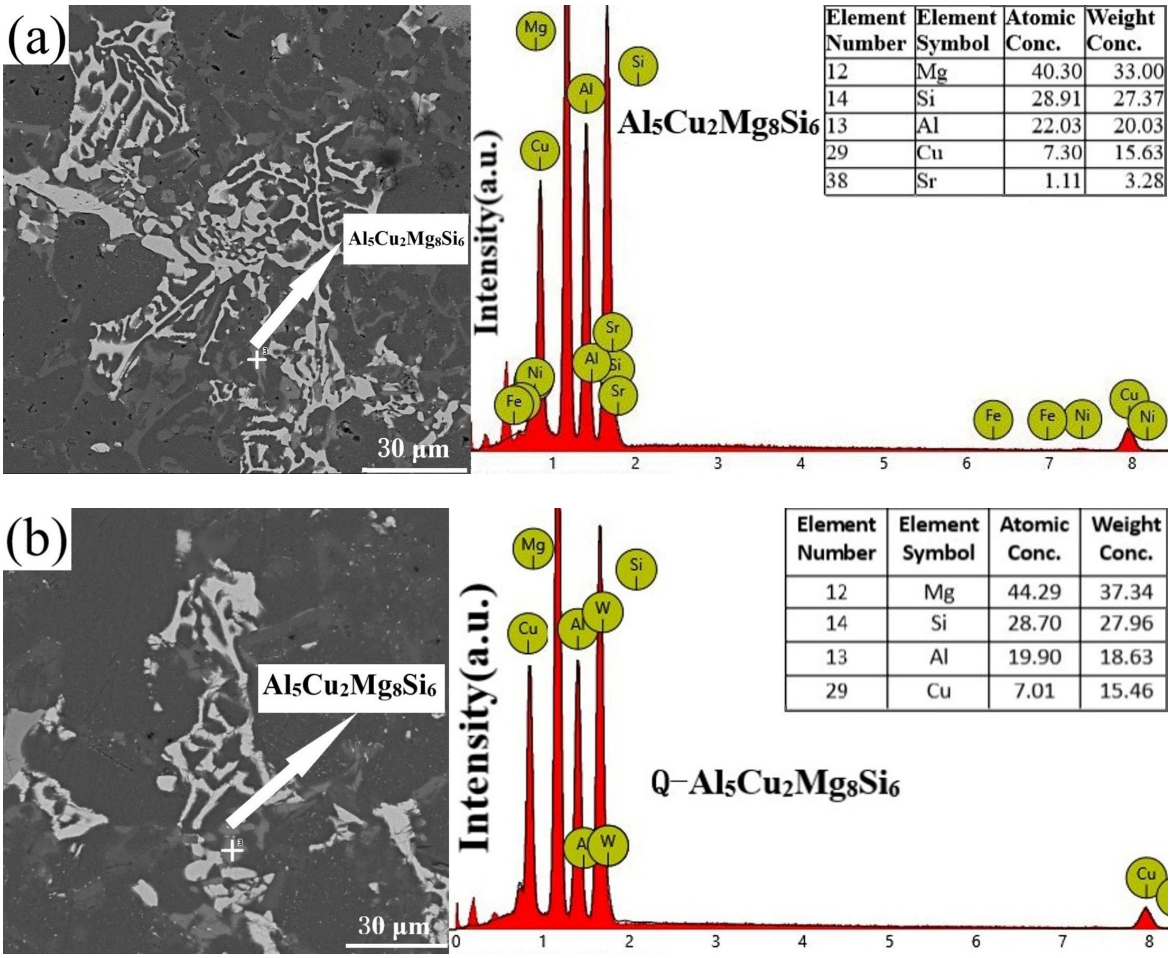


Figure 5. Fe phase scanning morphology (SEM) and energy dispersive spectroscopy (EDS) analysis of cast Al-Si alloy: (**a**) AlFeSiCuNi phase, (**b**) AlSiFeNi phase, and (**c**) AlSiCrFeNi phase.

The morphology of the eutectic Si of the alloys before and after thermal exposure at 350 °C was compared in Figure 9. As displayed in Figure 9, the eutectic Si of Alloy 1 existed in the form of rod-shaped aggregation with relatively sparse distribution. The eutectic Si in Alloy 2 and Alloy 3 existed in the form of network, which was relatively dense. The size of the eutectic Si of the three alloys demonstrated no evident difference. Compared with the eutectic Si in as-cast alloys, it was found that the size of eutectic Si showed obvious coarsening after thermal exposure. It was worth noting that under normal circumstances, the coarsening of the second phase would make its morphology more intensive. However, combined with the results of IPP analysis, the average size of eutectic Si increased after thermal exposure, while the mesh Si became sparse. The reason for the occurrence of this phenomenon was that fine rod-shaped eutectic Si dissolved and gradually disappeared, while coarse eutectic Si absorbed Si atoms and grew up during the thermal exposure, a process called Ostwald ripening [18].



Element Number	Element Symbol	Atomic Conc.	Weight Conc.
12	Mg	40.30	33.00
14	Si	28.91	27.37
13	Al	22.03	20.03
29	Cu	7.30	15.63
38	Sr	1.11	3.28

Element Number	Element Symbol	Atomic Conc.	Weight Conc.
12	Mg	44.29	37.34
14	Si	28.70	27.96
13	Al	19.90	18.63
29	Cu	7.01	15.46

Figure 6. Q phase scanning morphology (SEM) and energy dispersive spectroscopy (EDS) analysis of Al-Si alloy: (**a**) before thermal exposure, (**b**) after thermal exposure.

Figure 10 presents the average grain sizes of the as-cast alloys characterized using IPP software. As shown in Figure 10a, the mean sizes of eutectic Si in cast alloys were 3.82 μm, 4.18 μm, and 3.78 μm for studied alloys, respectively. It was found that the eutectic Si sizes of Alloy 1 to Alloy 3 displayed no significant change, indicating that the sizes of eutectic Si held steady when increasing the Fe.

Figure 10b displayed the average peak size distribution of the Fe-phase (take the Fe-phase with the largest size in 10 different metallographic diagrams to find the mean). By increasing the Fe from 0.3 (wt. %) to 0.9 (wt. %), the sizes of Fe-rich phases were 28 μm, 37.2 μm and 59 μm, respectively, which increased dramatically. The results of the IPP analysis showed that the sizes of the Fe phases increased as the Fe increased.

Figure 11 illustrates the average grain sizes of the studied alloys after thermal exposure. Figure 11a shows that the sizes of the Fe phases in TE (thermally exposed) state from Alloy 1 to Alloy 3 were 26.9 μm, 38.5 μm, 57.5 μm, respectively. Before thermal exposure, the sizes of the Fe phases were 28 μm, 37.2 μm, and 59 μm, respectively, which showed no apparent change, indicating that the Fe phases possessed excellent thermal stability at 350 °C. As shown in Figure 11b, the sizes of eutectic Si in the thermally exposed were coarsened sharply, and the mean sizes after thermal exposure were 5.3 μm, 5.4 μm, and 5.8 μm, respectively. The sizes of eutectic Si increased by 38.21%, 29.66%, and 52.91% compared with those before thermal exposure, respectively. The average particle sizes of varies phases before and after thermal exposure are shown in Table 3.

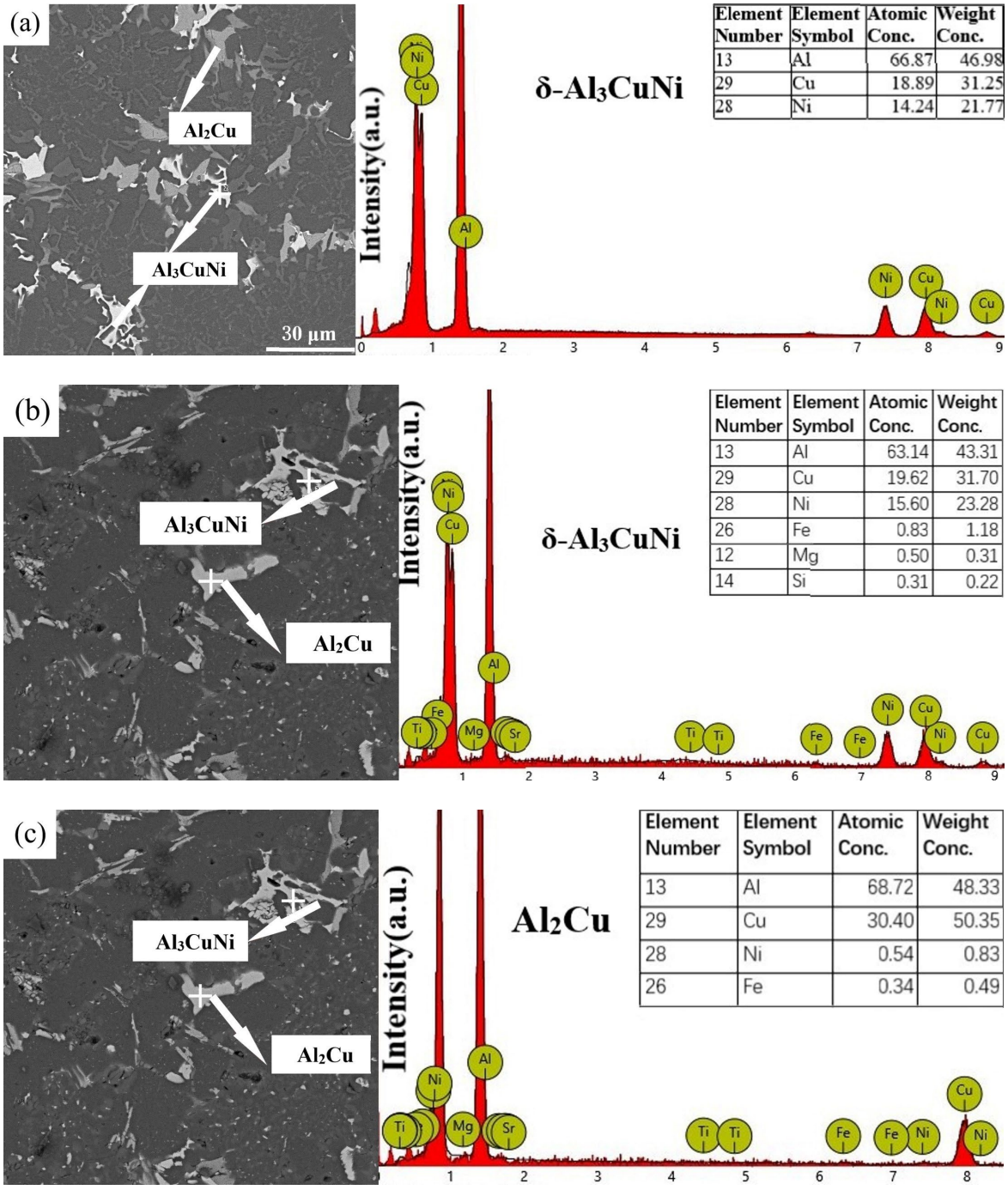


Figure 7. Scanning morphology and energy spectrum analysis of thermally exposed Al_3CuNi and Al_2Cu: (**a**) before thermal exposure, (**b**,**c**) after thermal exposure.

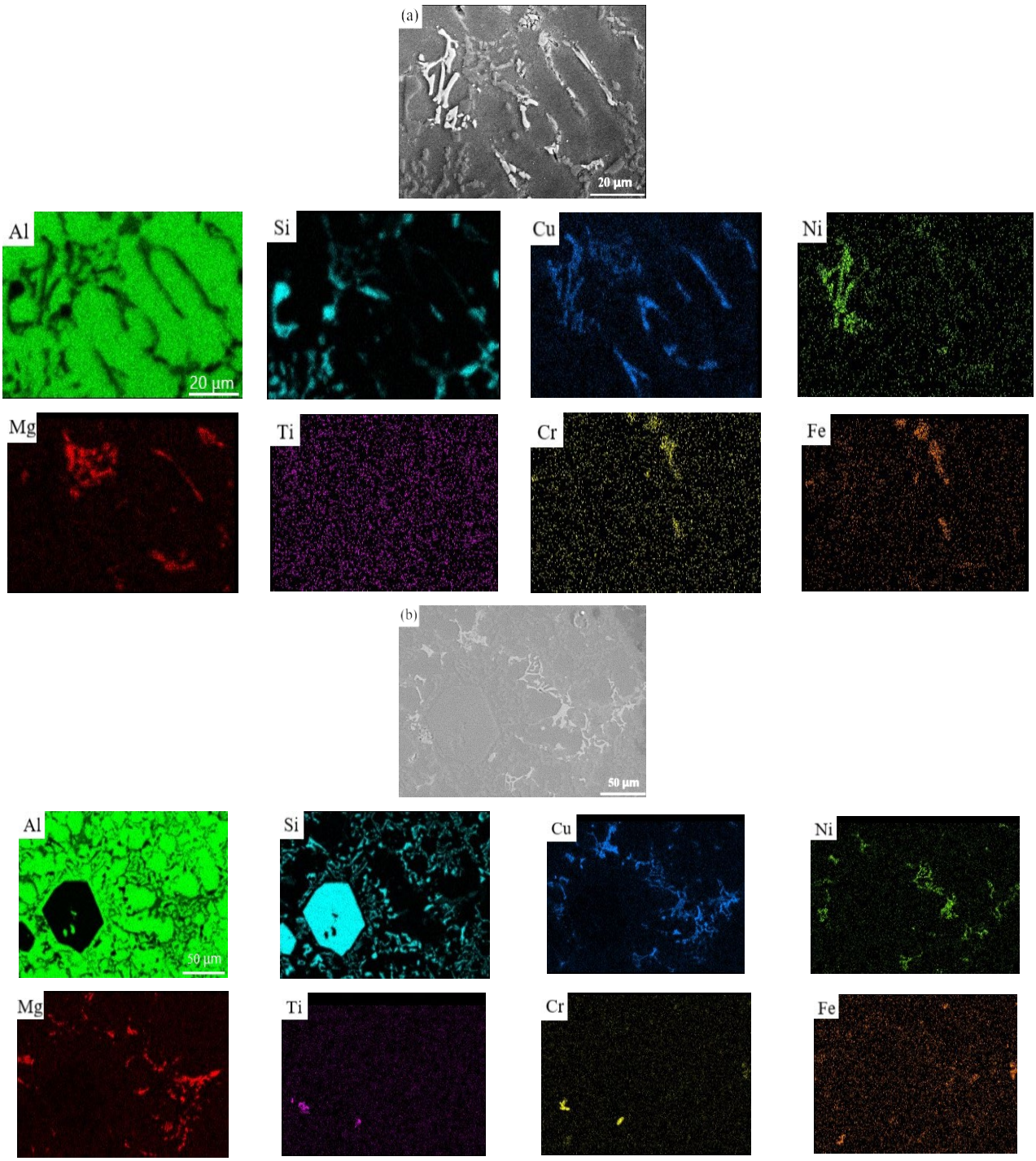


Figure 8. Scanning morphology (SEM) and surface scanning (Mapping) of cast Alloy 2: (**a**) as-cast, (**b**) after thermal exposure.

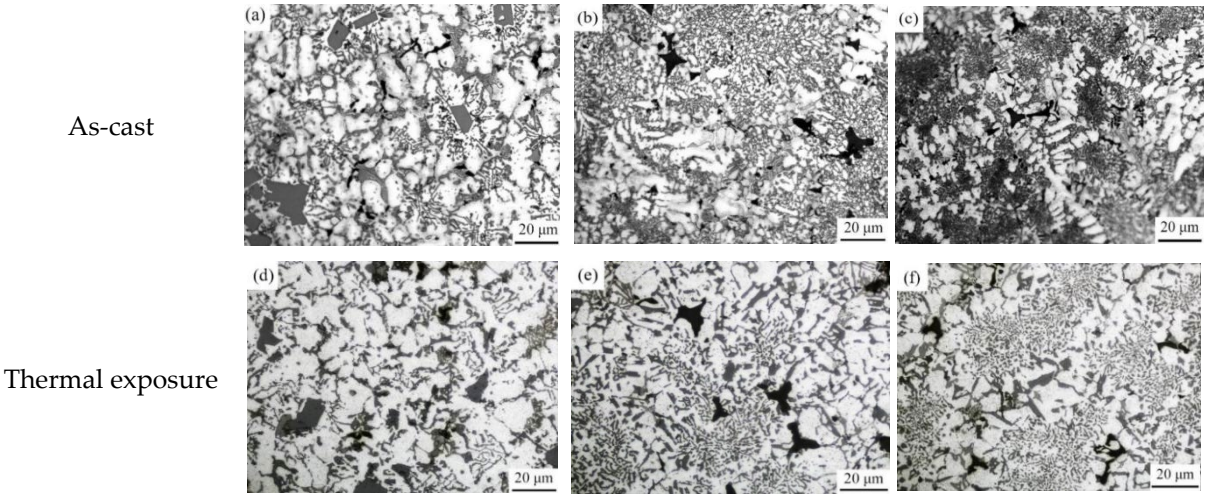


Figure 9. Metallographic morphology of eutectic Si before and after thermal exposure: (**a**,**d**) Alloy 1, (**b**,**e**) Alloy 2, and (**c**,**f**) Alloy 3.

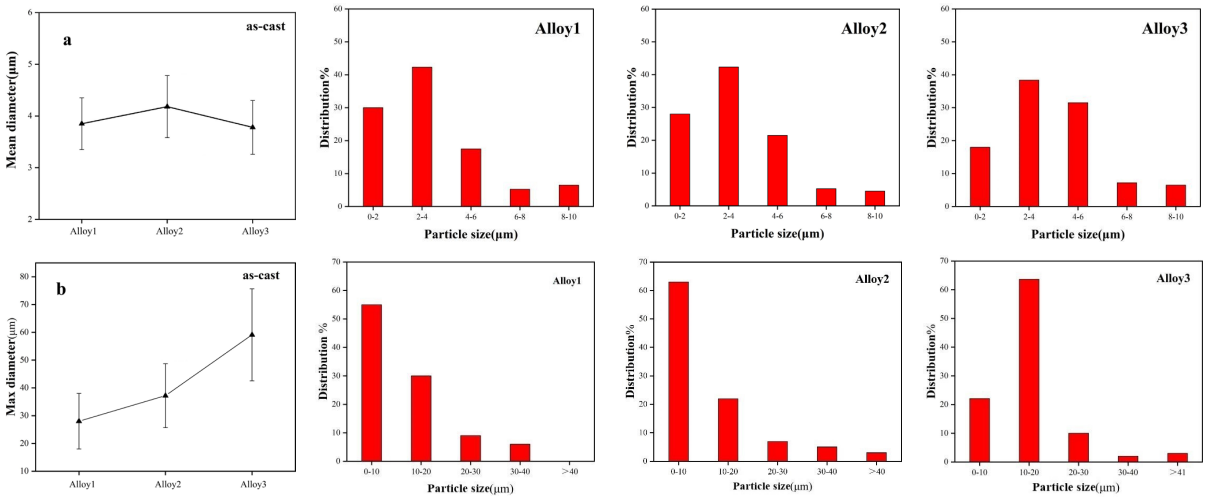


Figure 10. Average grain size in as-cast alloys: (**a**) eutectic Si, (**b**) Fe phase.

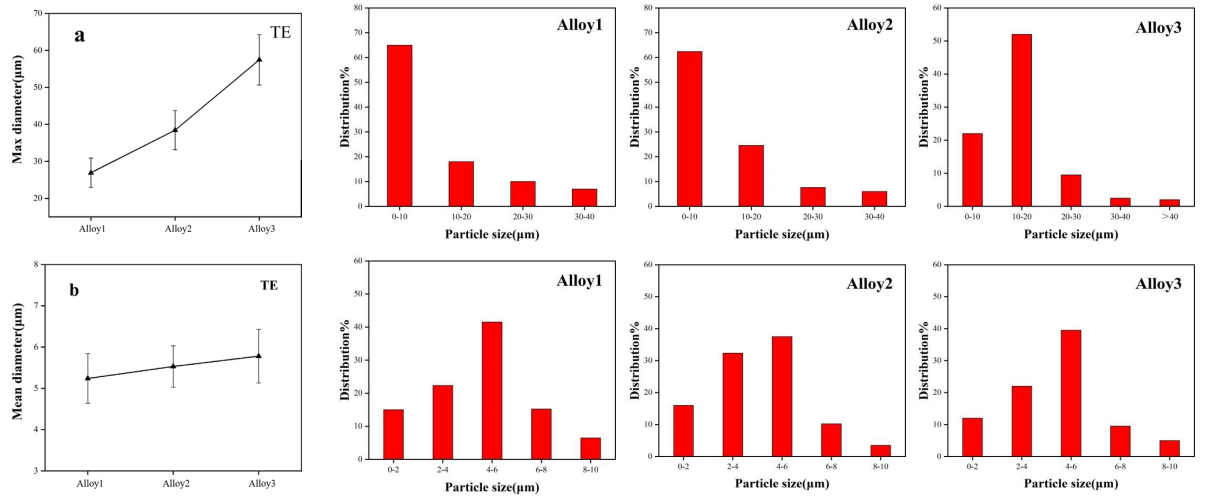


Figure 11. Average grain size of the alloys after thermal exposure: (**a**) Fe phase, (**b**) eutectic Si.

Table 3. Mean particle sizes of varies phases before and after thermal exposure.

Fe (wt. %) / Phases	As-Cast			After Thermal Exposure		
	0.3	**0.6**	**0.9**	**0.3**	**0.6**	**0.9**
Fe-rich	28.0 μm	37.2 μm	59.0 μm	26.9 μm	38.5 μm	57.5 μm
eutectic Si	3.8 μm	4.2 μm	3.8 μm	5.3 μm	5.5 μm	5.8 μm

The coarsening of eutectic Si occurred during thermal exposure at 350 °C. Since no additional Si atoms were added, there was no chemical driving force of eutectic Si. In addition, no elastic deformation occurred during the thermal exposure, and eutectic Si was not deformed through the action of molecular forces. Therefore, the coarsening power of eutectic Si was provided by the interfacial energy between the Al matrix and the second phase, indicating that the coarsening of eutectic Si was achieved by reducing the interfacial area. The ripening principle and analysis of eutectic Si are discussed as follows [19,20]:

The expression for Gibbs free energy was generalized as Equation (1):

$$G = V(G_v + G_e) + S_\gamma \tag{1}$$

where r is the radius of eutectic Si, V is the volume of eutectic Si, S is the phase interface energy, G_v is the free energy per unit volume, G_e is the elastic strain energy per unit volume, and γ is the specific surface energy and Ω is the molar volume.

The expression for the chemical potential of the solute is summarized as in Equation (2):

$$\mu = \Omega\frac{\partial G}{\partial V} = \Omega(G_v + G_e) + \Omega\left(\frac{\partial S}{\partial V}\right)\gamma \tag{2}$$

It was obtained via a simple conversion of Equation (2), as follows:

$$\mu = \Omega\frac{\partial G}{\partial V} = \Omega(G_v + G_e) + \frac{2\Omega\gamma}{2} \tag{3}$$

From Equation (3), it was found that the chemical potential of the solute was inversely proportional to the radius of eutectic Si, and the second phase particles and α-Al were in local equilibrium at the interface; therefore, the chemical potential of the solute atom was equal to the chemical potential of the second phase particles. It was assumed that there were two particles in the α-Al matrix, whose sizes were r_1 and r_2 ($r_1 > r_2$); therefore, the chemical potential gradient Δμ was established in α-Al between two different eutectic Si, and the expression was generalized as in Equation (4):

$$\Delta\mu = \mu_2 - \mu_1 = 2\Omega\gamma\left(\frac{1}{r2} - \frac{1}{r1}\right) \tag{4}$$

The schematic diagram of the Ostwald ripening process mechanism is illustrated in Figure 12. Driven by Δμ, in order to achieve the equilibrium between particles and the Al matrix, the solute atoms escaped from the small-sized particles that tended to diffuse to the large-sized particles, resulting in the solute atom concentration near the small-sized particles being smaller than the equilibrium concentration. In order to maintain the equilibrium at the interface, the small-sized particles continue to dissolve, while the large-sized particles continue to grow, which is called the Ostwald ripening phenomenon.

The dense network eutectic Si distributed in the Al matrix represented a certain hindrance to the dislocation movement in the alloy, which was beneficial to the mechanical properties of the alloy, whereas the network eutectic Si coarsened; meanwhile, the microstructure became more sparser after thermal exposure. The hindrance to dislocation movement had been reduced, with the dislocation climbing and cross slipping in the alloy were released to a certain extent. Therefore, the performance of the alloy decreased observably after thermal exposure at 350 °C for 200 h. Hence, it was necessary to use

IPP software to carry out statistical analysis on the coarsening degree of eutectic Si after thermal exposure.

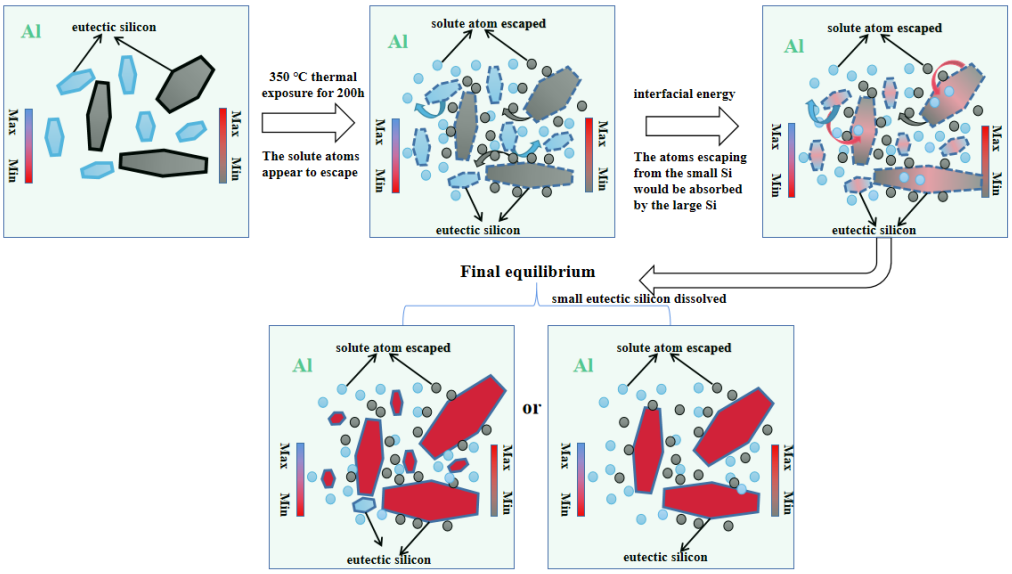


Figure 12. Schematic diagram of the Ostwald ripening process mechanism.

3.2. Mechanical Properties

Figure 13 presents the ultimate tensile strength (UTS) and elongation of the cast alloy at 350 °C. The UTS of Alloy 1 to Alloy 3 alloy was 111.2 MPa, 124 MPa and 128.7 MPa, respectively. Large-sized Fe phase can be served as an elevated-resistant phase in elevated temperature. Hence, the dislocation motion inside the alloy was hindered, and the tensile strength of the alloy at an elevated temperature improved. Fe increased from 0.3 (wt. %) to 0.9 (wt. %), the Fe phase size increased obviously, and the performance at elevated temperature of the alloy improved to a certain extent. In conclusion, the performance at elevated temperature increased with the increase in Fe.

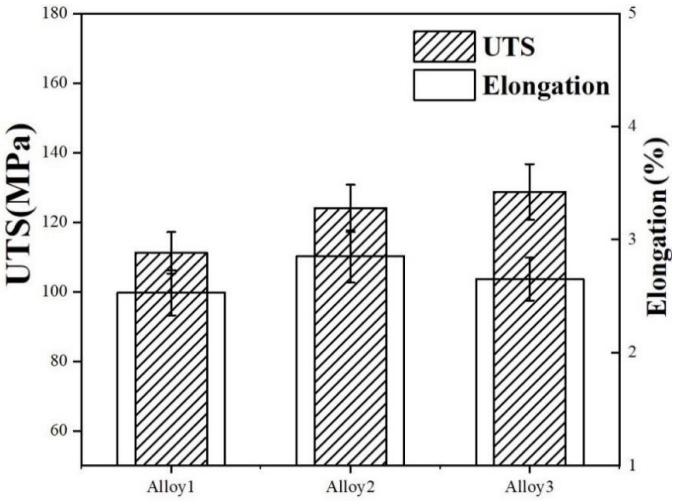


Figure 13. Tensile strength and elongation of cast Al-Si alloy tested at 350 °C.

From Alloy 1 to Alloy 3, the elongations at elevated temperature were 2.53%, 2.85%, and 2.65%, respectively. Compared with the casting state, the elongation was greatly increased because the Al matrix would soften at 350 °C; in addition, it tended to be ductile during the elevated temperature tensile process, which dramatically improved

the plasticity of the alloy. The stress between the reinforced phases and the matrix also decreased; therefore, the elongation increased significantly compared with the casting state.

Figure 14 illustrates the UTS and elongation of the thermally exposed alloy at 350 °C. The UTS at 350 °C of Alloy 1–Alloy 3 was 84.5 MPa, 96.7 MPa and 98.8 MPa, respectively, which decreased by 24%, 22.1% and 23.23% compared with 111.2 MPa, 124 MPa and 128.7 MPa in the casting state. The elongations after thermal exposure were 2.8%, 3.05% and 3.15%, respectively, which were slightly higher than those in the casting state.

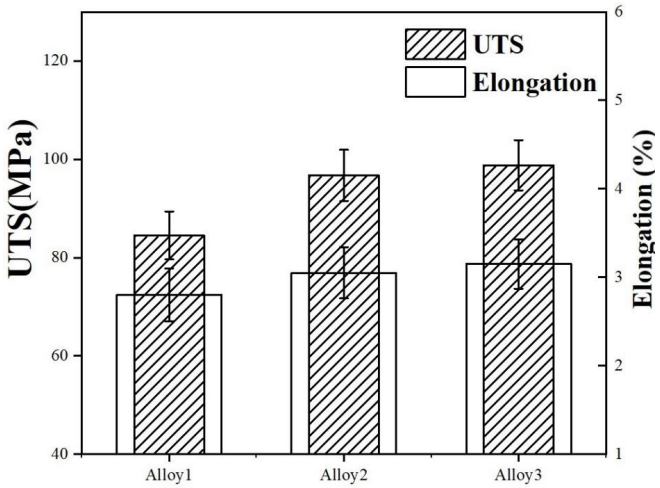


Figure 14. Tensile strength and elongation of thermally exposed Al-Si alloy tested at 350 °C.

From the hardness curve in Figure 15, it was found that the hardness of Alloy 3 rapidly dropped from HV147.64 to HV105.1 at the initial stage of thermal exposure (0.5 h), with a decrease of 28.9%. With the increase in thermal exposure time, the hardness became stable at approximately 32 h, and reached HV75 after 200 h of thermal exposure. The hardness of Alloy2 decreased to HV90.72 after thermal exposure at 350 °C for 0.5 h, with a decrease of 22.5%, and tended to be stable around 32 h, with a decrease of 8.1% compared with Alloy 3. The hardness of Alloy 1 changed from HV120 to HV65.6 after thermal exposure at 350 °C for 200 h, with a decrease of 45.3%. The hardness of Alloy 1 essentially stabilized after thermal exposure for 64 h. The hardness of the three alloys declined sharply at the initial stage of thermal exposure (0.5~8 h), and gradually stabilized during the subsequent thermal exposure process.

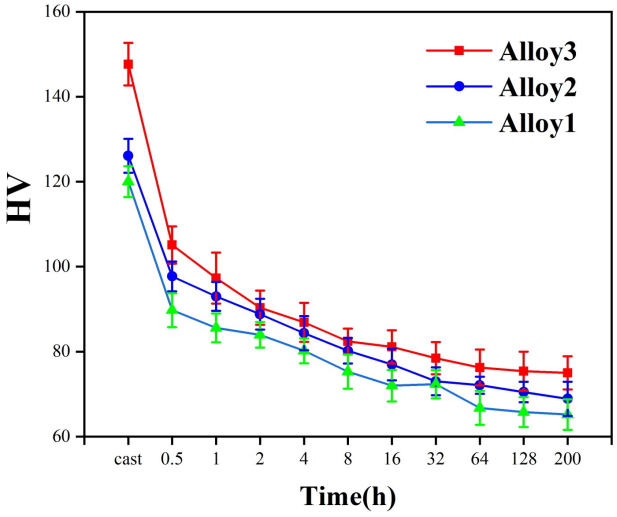


Figure 15. Hardness evolution of Al-Si alloy at room temperature after thermal exposure at 350 °C for various times.

It is worth noting that the hardness of alloy decreased dramatically at the initial stage of thermal exposure (0.5 h). The reason for this phenomenon may be that there were many alloying elements with intricate compositions, and the supersaturated solid solution formed by these alloying elements would produce lattice distortion, which triggered a long-range stress field. There was a significant number of dislocations in the alloy and the movement of dislocations between crystal particles had to overcome the effect of the stress field. At the initial stage of thermal exposure, the internal stress of the alloy declined, which weakened the hindrance effect of the stress field on dislocations. Therefore, the dislocations received a certain degree of increase, resulting in the hardness decreasing significantly. It was speculated that the alloy hardness declined with the extension of time because the long-term thermal exposure led the grain to grow and coarsen, and the dissolution of the strengthened phase or the increase in metastable phase precipitated, which led to the decrease in the alloy's resistance to plastic deformation.

Figure 16 presents the UTS of the alloys after thermal exposure at room temperature. The UTS of Alloy 1 after thermal exposure decreased from 249.2 MPa to 170.3 MPa with a decrease of 31.66%, which is consistent with relevant research conclusions [13]. The UTS of Alloy 2 decreased dramatically at the stage of thermal exposure for 0.5~8 h, and the stable tensile strength was 140.2 MPa, which decreased by 30.39%. The UTS of Alloy 3 showed a significant decrease in the initial stage of thermal exposure. The UTS tended to be stable at 64 h and the stable tensile strength was 125.3 MPa; compared with the cast strength, the decrease was of 28.07%.

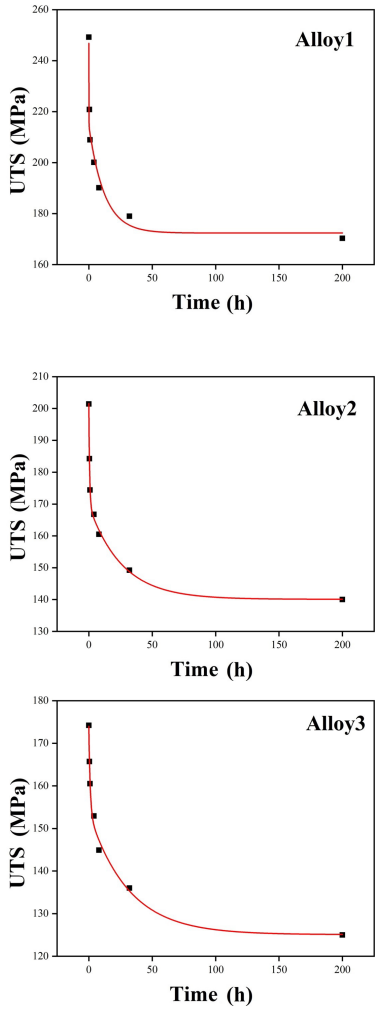


Figure 16. Ultimate tensile strength and fitted curves of Al-Si alloy after thermal exposure at 350 °C for different time.

The decrease in ultimate tensile strength of the studied alloys was, from Alloy 1 to Alloy 3, 31.66%, 30.39% and 28.07%, respectively, suggesting that the resistance of the reduction in UTS was improved with increasing the Fe.

Figure 17 displayed the SEM images of the tensile fracture of different alloys at room temperature. It is observed in Figure 11a that there were a great number of flat cleavage planes in the fracture, indicating that the fracture was generated at the primary Si. Therefore, the fracture type of Alloy 1 was a typical transgranular brittle fracture, and the fracture mechanism was cleavage fracture. Figure 11b shows the fracture of Alloy 2 at room temperature. With the increase in Fe, the number of large-area cleavage planes at the fracture surface declined, and more small-area cleavage planes appeared. The fracture occurred at the coarse eutectic silicon, and the fracture mechanism was cleavage fracture. There were a large number of cleavage plane platforms and it was observed that cracks were generated by strengthening the interaction in Alloy 3, indicating that the fracture of the second phase led to the final fracture failure, which is consistent with the relevant research results [21]. Hence, the fracture type was a transgranular brittle fracture, and the fracture mechanism was cleavage fracture.

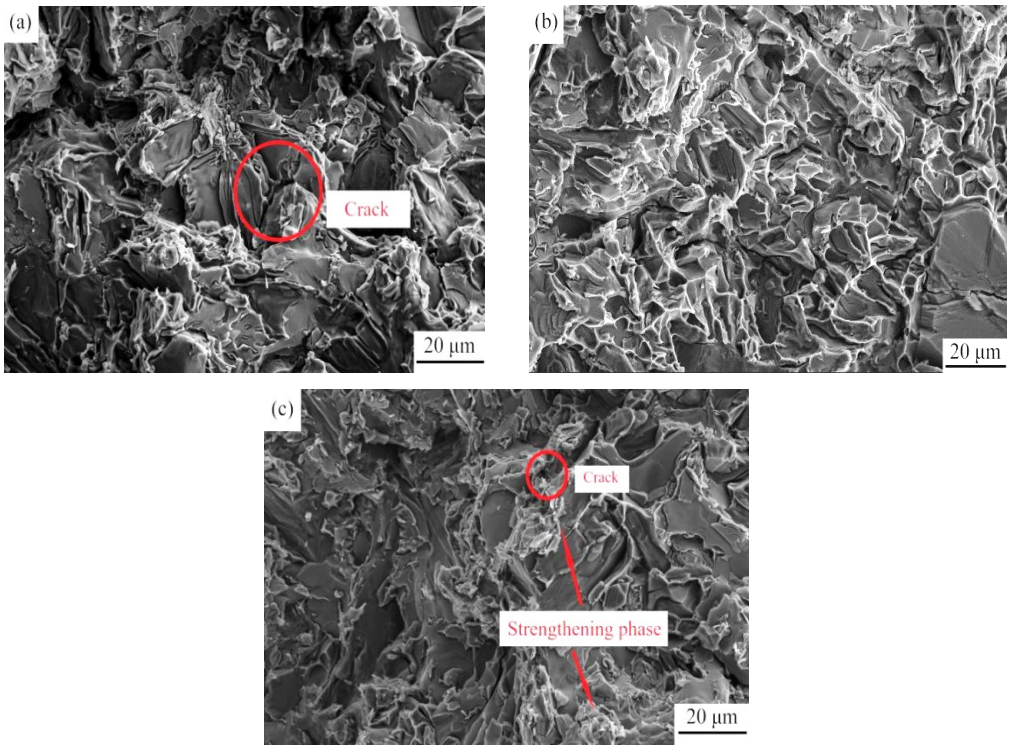


Figure 17. Scanning electron microscopy on fracture of cast Al-Si alloy at room temperature: (**a**) Alloy 1, (**b**) Alloy 2, and (**c**) Alloy 3.

The SEM images of the fracture of the cast Al-Si alloy at an elevated temperature are illustrated in Figure 18. The tensile fracture at an elevated temperature was obviously different from that at room temperature. The Al matrix would soften to a greater extent at elevated temperature. Therefore, the Al matrix possessed good ductility, and obvious plastic deformation occurred while tensile at an elevated temperature, which manifested as a large number of dimples distributed on the fracture surface. The coarse Fe phase possessed higher hardness and served as a heat-resistant phase at an elevated temperature, which effectively prevented dislocation and slip, leading to the elevated temperature strength of the matrix being greatly improved. The fractures of the three alloys were all composed of dimples and cleavage planes, indicating that the fracture mode of the alloys with different Fe elements at an elevated temperature was a ductile fracture, and the fracture mechanism changed to quasi-cleavage fracture.

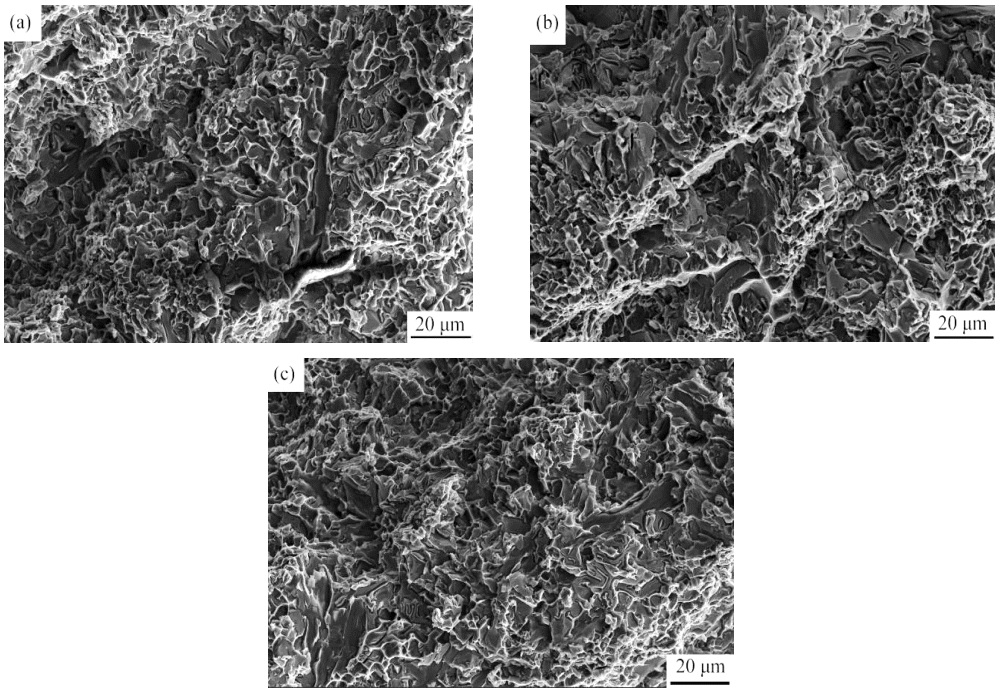


Figure 18. Scanning electron microscopy on fracture of cast Al-Si alloy at elevated temperature: (**a**) Alloy 1, (**b**) Alloy 2, and (**c**) Alloy 3.

4. Conclusions

The effects of thermal exposure and Fe on the mechanical properties of Al-Si-Cu-Ni-Mg-(0.6–0.9%) Fe (wt. %) alloy have been investigated in the present work. The main conclusions of this study can be generalized as follows:

1. The main phases of the Al-Si-Cu-Ni-Mg-Fe alloys at room temperature were the α-Al, Si, $Al_5Cu_2Mg_8Si_6$, Al_3CuNi, Al_7Cu_4Ni, Al_2Cu, and AlFeSi phases.
2. The size of AlSiFe phase increased with the increase in Fe. The shape of the Fe-rich phase changed from rod-like to star-like, followed by a long needle shape, with Fe varying from 0.6% to 0.9%.
3. The ductility and strength of the studied alloys decreased with increasing Fe at room temperature. The mechanical properties of the studied alloys increased with Fe at an elevated temperature, indicating that the Fe-rich phase has great potential for the development of high strength and toughness heat-resistant aluminum.
4. Eutectic Si coarsened after thermal exposure, whereas the microstructure was sparser, which was caused by Ostwald ripening, resulting in a decreased performance after thermal exposure.
5. The UTS and HV of the studied alloys decreased dramatically at 0.5~8 h and then tended to be stable after thermal exposure at 350 °C for approximately 64 h.

Author Contributions: Conceptualization, J.L. and L.Z.; methodology, L.Z.; software, Y.W.; validation, L.Z.; formal analysis, F.C.; investigation, J.L.; resources, Y.Z.; data curation, Y.H.; writing—original draft preparation, R.Z.; writing—review and editing, F.C.; visualization, Y.L.; supervision, K.S.; project administration, R.Z.; funding acquisition, L.Z. All authors have read and agreed to the published version of the manuscript.

Funding: This work was funded by the Natural Science Foundation of the Jiangsu Higher Education Institutions of China (grant number 20KJB430015), the Open Fund of Jiangsu Institute of Marine Resources Development (grant number JSIMR202208), Jiangsu Province Special Project for the Transformation of Scientific and Technological Achievements (grant number BA2022059).

Conflicts of Interest: The authors declare no conflict of interest.

References

1. Meng, F.; Wu, Y.; Hu, K.; Li, Y.; Sun, Q.; Liu, X. Evolution and Strengthening Effects of the Heat-Resistant Phases in Al-Si Piston Alloys with Different Fe/Ni Ratios. *Materials* **2019**, *12*, 2506. [CrossRef] [PubMed]
2. Yang, Y.; Zhong, S.-Y.; Chen, Z.; Wang, M.; Ma, N.; Wang, H. Effect of Cr content and heat-treatment on the elevated temperature strength of eutectic Al-Si alloys. *J. Alloys Compd.* **2015**, *647*, 63–69. [CrossRef]
3. Feng, J.; Ye, B.; Zuo, L.; Qi, R.; Wang, Q.; Jiang, H.; Huang, R.; Ding, W. Effects of Ni content on low cycle fatigue and mechanical properties of Al-12Si-0.9Cu-0.8Mg-xNi at 350 °C. *Mater. Sci. Eng. A* **2017**, *706*, 27–37. [CrossRef]
4. Chen, F.; Liu, C.; Zuo, L.; Wu, Z.; He, Y.; Dong, K.; Li, G.; He, W. Effect of Thermal Exposure on Mechanical Properties of Al-Si-Cu-Ni-Mg Aluminum Alloy. *Crystals* **2023**, *13*, 236. [CrossRef]
5. Li, Y.; Yang, Y.; Wu, Y.; Wei, Z.; Liu, X. Supportive strengthening role of Cr-rich phase on Al-Si multicomponent piston alloy at elevated temperature. *Mater. Sci. Eng. A* **2011**, *528*, 4427–4430. [CrossRef]
6. Jung, J.-G.; Lee, S.-H.; Cho, Y.-H.; Yoon, W.-H.; Ahn, T.-Y.; Ahn, Y.-S.; Lee, J.-M. Effect of transition elements on the microstructure and tensile properties of Al-12Si alloy cast under ultrasonic melt treatment. *J. Alloys Compd.* **2017**, *712*, 277–287. [CrossRef]
7. Zuo, L.; Ye, B.; Feng, J.; Xu, X.; Kong, X.; Jiang, H. Effect of δ-Al_3CuNi phase and thermal exposure on microstructure and mechanical properties of Al-Si-Cu-Ni alloys. *J. Alloys Compd.* **2019**, *791*, 1015–1024. [CrossRef]
8. Farkoosh, A.R.; Pekguleryuz, M. Enhanced mechanical properties of an Al-Si-Cu-Mg alloy at 300 °C: Effects of Mg and the Q-precipitate phase. *Mater. Sci. Eng. A* **2015**, *621*, 277–286. [CrossRef]
9. Li, G.; Liao, H.; Suo, X.; Tang, Y.; Dixit, U.S.; Petrov, P. Cr-induced morphology change of primary Mn-rich phase in Al-Si-Cu-Mn heat resistant aluminum alloys and its contribution to elevated temperature strength. *Mater. Sci. Eng. A Struct. Mater. Prop. Misrostruct. Process.* **2018**, *709*, 90–96. [CrossRef]
10. Zhang, J.Y.; Zuo, L.J.; Feng, J.; Ye, B.; Kong, X.Y.; Jiang, H.Y.; Ding, W.J. Effect of thermal exposure on microstructure and mechanical properties of Al-Si-Cu-Ni-Mg alloy produced by different cast technologies. *Trans. Nonferrous Met. Soc. China* **2020**, *30*, 1717–1730. [CrossRef]
11. Abdelaziz, M.H.; Doty, H.W.; Valtierra, S.; Samuel, F.H. Static versus dynamic thermal exposure of transition elements-containing Al-Si-Cu-Mg cast alloy. *Mater. Sci. Eng. A* **2018**, *739*, 499–512. [CrossRef]
12. Zhao, B.; Ye, B.; Wang, L.; Bai, Y.; Yu, X.; Wang, Q.; Yang, W. Effect of ageing and thermal exposure on microstructure and mechanical properties of a HPDC Al–Si–Cu–Mg alloy. *Mater. Sci. Eng. A* **2022**, *849*, 143463. [CrossRef]
13. Lin, B.; Li, H.; Xu, R.; Zhao, Y.; Xiao, H.; Tang, Z.; Li, S. Thermal exposure of Al-Si-Cu-Mn-Fe alloys and its contribution to high temperature mechanical properties. *J. Mater. Res. Technol.* **2020**, *9*, 1856–1865. [CrossRef]
14. Asghar, Z.; Requena, G.; Kubel, F. The role of Ni and Fe aluminides on the elevated temperature strength of an AlSi12 alloy. *Mater. Sci. Eng. A* **2010**, *527*, 5691–5698. [CrossRef]
15. Asghar, Z.; Requena, G.; Boller, E. Three-dimensional rigid multiphase networks providing elevated-temperature strength to cast AlSi10Cu5Ni1-2 piston alloys. *Acta Mater.* **2011**, *59*, 6420–6432. [CrossRef]
16. Farkoosh, A.R.; Chen, X.G.; Pekguleryuz, M. Dispersoid strengthening of a high temperature Al-Si-Cu-Mg alloy via Mo addition. *Mater. Sci. Eng. A* **2015**, *620*, 181–189. [CrossRef]
17. Xiao, D.H.; Wang, J.N.; Ding, D.Y.; Chen, S.P. Effect of Cu content on the mechanical properties of an Al-Cu-Mg-Ag alloy. *J. Alloys Compd.* **2002**, *343*, 77–81. [CrossRef]
18. Zuo, L.; Ye, B.; Feng, J.; Zhang, H.; Kong, X.; Jiang, H. Effect of ε-Al_3Ni phase on mechanical properties of Al-Si-Cu-Mg-Ni alloys at elevated temperature. *Mater. Sci. Eng. A* **2020**, *772*, 138794. [CrossRef]
19. Zuo, L.; Ye, B.; Feng, J.; Bao, Q.; Kong, X.; Jiang, H.; Ding, W. Phases formation and evolution at elevated temperatures of Al-12Si-3.8Cu-2Ni-0.8Mg alloy. *Adv. Eng. Mater.* **2017**, *19*, 1–8. [CrossRef]
20. Zuo, L.; Ye, B.; Feng, J.; Kong, X.; Jiang, H.; Ding, W. Effect of Q-$Al_5Cu_2Mg_8Si_6$ phase on mechanical properties of Al-Si-Cu-Mg alloy at elevated temperature. *Mater. Sci. Eng. A* **2017**, *693*, 26–32. [CrossRef]
21. Jiao, X.Y.; Liu, C.F.; Guo, Z.P.; Tong, G.D.; Ma, S.L.; Bi, Y.; Zhang, Y.F.; Xiong, S.M. The characterization of Fe-rich phases in a high-pressure die cast hypoeutectic aluminum-silicon alloy. *J. Mater. Sci. Technol.* **2020**, *51*, 54–62. [CrossRef]

Disclaimer/Publisher's Note: The statements, opinions and data contained in all publications are solely those of the individual author(s) and contributor(s) and not of MDPI and/or the editor(s). MDPI and/or the editor(s) disclaim responsibility for any injury to people or property resulting from any ideas, methods, instructions or products referred to in the content.